Iron Oxychalcogenides and Their Photocurrent Responses

Sandy Al Bacha, Sébastien Saitzek, Houria Kabbour, Emma Mccabe

Iron oxychalcogenides and their photocurrent responses

Sandy Al Bacha[a,b,c], Sébastien Saitzek[d], Houria Kabbour[a, e]*, Emma E. McCabe[c]*

[a] Univ. Lille, CNRS, Centrale Lille, ENSCL, Univ. Artois, UMR 8181 – UCCS – Unité de Catalyse et Chimie du Solide, F-59000 Lille, France
[b] University of Kent, School of Physical Sciences, Canterbury, Kent CT2 7NH, U.K
[c] Durham University, Departement of Physics, Durham DH1 3LE, U.K.
[d] Univ. Artois, CNRS, Centrale Lille, Univ. Lille, UMR 8181, Unité de Catalyse et Chimie du Solide (UCCS), F-62300 Lens, France.
[e] Nantes Université, CNRS, Institut des Matériaux de Nantes Jean Rouxel – UMR6502, F-44000, Nantes, France

Corresponding authors: houria.kabbour@cnrs-imn.fr ; emma.mccabe@durham.ac.uk

Abstract:

We report here the results of an experimental investigation of the electronic properties and photocurrent responses of CaFeO*Q* and $La_2O_2Fe_2OQ_2$ phases, and a computational study of the electronic structure of polar CaFeOSe. We find that both CaFeO*Q* (*Q* = S, Se) have band gaps and conduction band edge positions compatible with light-driven photocatalytic water splitting, although the oxysulfide suffers from degradation due to oxidation of Fe^{2+} sites. The higher O:*Q* ratio in the Fe^{2+} coordination environment in CaFeOSe increases its stability without increasing the band gap beyond the visible range. The photocurrent CaFeOSe shows fast electron – hole separation, consistent with calculated carrier effective masses. These results suggest that these iron oxychalcogenides warrant further study, to optimize their stability and morphology for photocatalytic and other photoactive applications.

Introduction:

Water splitting photocatalysis reactions have the potential to generate hydrogen in a clean and sustainable way if they can be carried out under solar irradiation. However, this imposes constraints on the magnitude of the photocatalyst's band gap 1.23 – 3.00 eV) and the band edge positions (conduction band minimum (CBM) more negative band than the reduction potential of H_2O/H_2 (0 V); valence band maximum (VBM) more positive than the oxidation potential of O_2/H_2O (1.23 V)).[1] Despite being stable and often straightforward to synthesize, many oxide photocatalysts have band gaps that are too large for excitation by visible light (e.g. TiO_2 (3 eV)[2], ZnO (3.2 eV[3]). On the other hand, although sulfides typically have smaller band gaps, they are often unstable (suffering sulfur self-oxidation) in the catalysis reaction conditions.[4]

One strategy to design new photocatalysts for water splitting under visible light is to consider mixed-anion materials,[5] and the ability to reduce the band gap by replacing some oxide ions by softer chalcogenide ions (e.g. S^{2-}, Se^{2-}) has motivated research into oxychalcogenides for photocatalytic applications. Several p block oxychalcogenides (e.g. $Sr_6Cd_2Sb_6O_7Q_{10}$ (*Q* = S, Se),[6, 7] $LaOInS_2$[8, 9]) and d^0 transition metal oxychalcogenides ($Sm_2Ti_2S_2O_5$,[10] $Y_2Ti_2O_5S_2$ [11]) have shown promising

properties for photocatalytic applications. In an effort to widen the landscape of transition metal oxychalcogenides for photoactive behavior (including photocatalysis, photovoltaicity),[12-14] we investigated some Fe^{2+} (d^6) oxychalcogenides to assess their potential for photoactivity including light-driven water splitting photocatalysis. The quaternary oxychalcogenides CaFeO*Q* adopt layered crystal structures with heteroleptic Fe^{2+} coordination environments and with their polar crystal structures (suggested to enhance electron-hole separation and photocatalytic performance),[15-17] seemed promising candidates for photoelectrochemical reactions.

CaFeOS crystallizes in a polar, non-centrosymmetric structure of $P6_3mc$ symmetry. Its layered structure consists of alternating layers of Ca^{2+} ions, and corner-linked $FeOS_3$ tetrahedra (Figure 1).[18-20] These heteroleptic polar units are packed with their dipoles parallel to the hexagonal axis, isostructural with CaZnOS.[21, 22] The photovoltaic activity proposed[23] for this semiconductor may suggest some promise for photocatalysis. The related oxyselenide CaFeSeO adopts a different structure, composed of puckered layers of corner-linked FeO_2Se_2 tetrahedra separated by layers of Ca^{2+} ions (Figure 1).[24, 25] Two polymorphs are known, which differ in the orientation of the polar FeO_2Se_2 units: a polar polymorph of $Cmc2_1$ symmetry with in-plane polarization,[25] and a non-polar, centrosymmetric polymorph of $Pmcn$ symmetry.[24] CaFeOSe is a strongly-correlated semiconductor and the non-polar polymorph is reported to have an indirect band gap of 1.8 eV.[24] Our attempts to prepare samples of the non-polar $Pmcn$ polymorph were successful and so the non-polar $La_2O_2Fe_2OQ_2$ phases were used for comparison. They also adopt layered crystal structures, but with quite different Fe^{2+} coordination, consisting of face-shared FeO_2Q_4 octahedra with 180° Fe – O – Fe connectivity.[26] These Mott insulating phases have narrow band gaps.[27] This comparison between CaFeO*Q* and $La_2O_2Fe_2OQ_2$ phases allows an investigation of the impact of the oxychalcogenide environment around Fe^{2+} cations on the band dispersion and therefore carrier effective masses and mobilities, key features for designing photoactive functional materials.

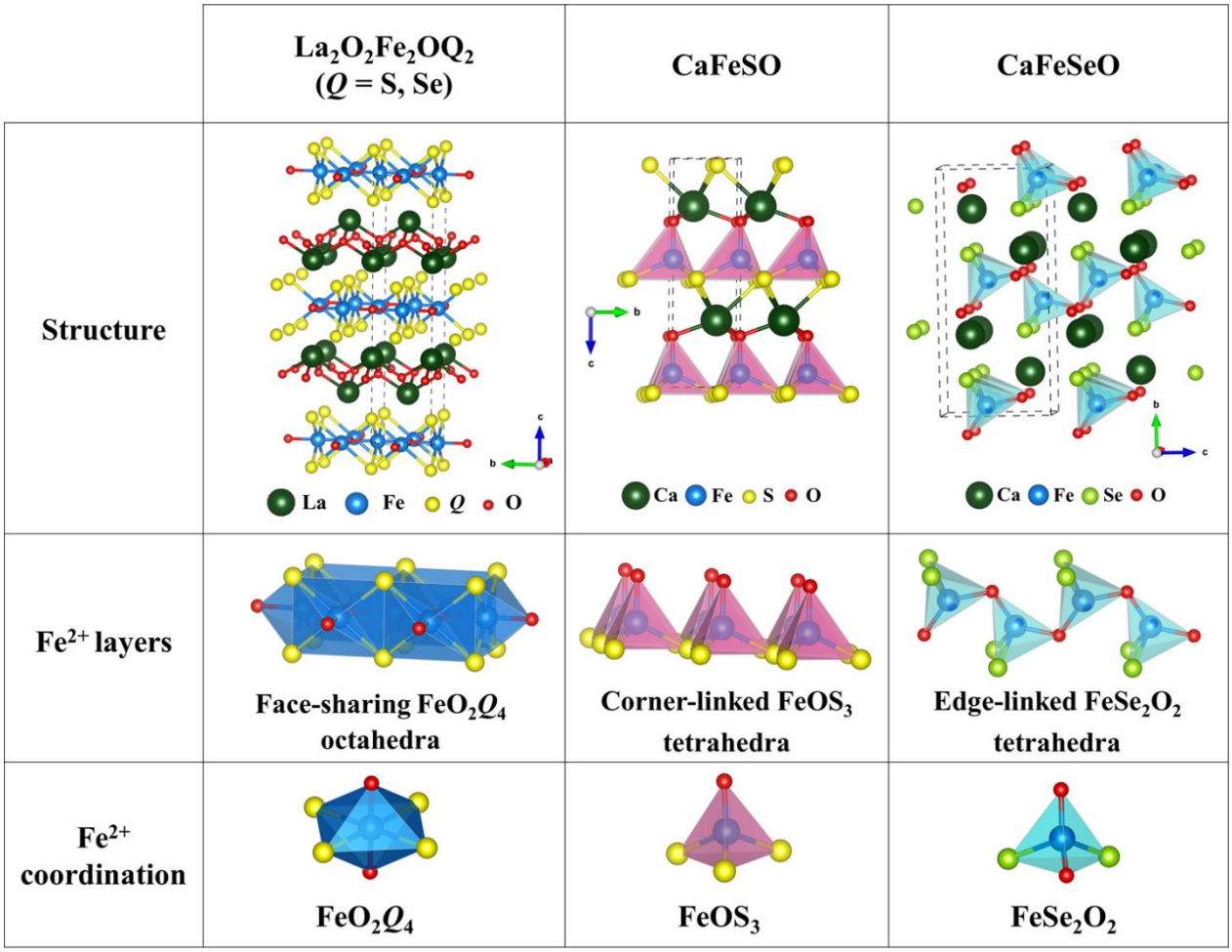

Figure 1 Overview of the crystal structures, Fe^{2+} layers and coordination environments for $La_2O_2Fe_2OQ_2$ and CaFeO*Q* (*Q* = S, Se) phases.

We report here the results optical and photocurrent measurements on CaFeO*Q* and $La_2O_2Fe_2OQ_2$ phases, and a density functional theory (DFT) calculation of the electronic structure of polar CaFeOSe and its charge carriers effective masses. A photocurrent response was measured for all materials, although the oxysulfide CaFeOS suffers from degradation. The photocurrent response for CaFeSeO indicated fast electron – hole separation, and recombination and transfer rates were calculated for this oxyselenide. Further studies on CaFeO*Q* (*Q* = S, Se) materials to optimize their stability would be interesting for potential photocatalytic materials.

Methods:

$La_2O_2Fe_2OQ_2$ and CaFeO*Q* (*Q* = S, Se) were prepared by solid-state reactions in evacuated, sealed, quartz tubes. Reagents were stored and manipulated in an argon-filled glovebox. For $La_2O_2Fe_2OQ_2$ (*Q* = S, Se) (0.5 g) analogues, La_2O_3, Fe and S/Se in the molar ratio 2:2.1:2 were used and the heat treatment consisted of heating to 400°C (1.5°C/min) for 12 h, and then heated to 600 °C (0.5°C/min) and then 850 °C for 12h. For CaFeO*Q* (*Q* = S, Se) (0.5 g) analogues, a mixture of the precursors CaO, Fe and Se/S in the molar ratio 1:1.05:1 was used. The heat treatment consisted of heating to 750°C at a rate of 5 °C/min for 60 h before quenching the sample for the oxyselenide, and heating to 950°C (0.5°C/min) for 24 h for the oxysulfide.

X-ray powder diffraction (XRPD) data were collected on a Bruker D8 A25 diffractometer equipped with a Lynxeye XET linear detector (Cu Kα) in Bragg−Brentano geometry at room temperature with a 1 s counting time and 0.02 ° step angle. Rietveld refinements using XRPD data were carried out

using Fullprof software.[28] The background, sample height, lattice parameters, peak profiles, atomic positions and atomic displacement parameters were refined. Vesta software[29] was used to visualize the crystal structure.

The reflectance of the CaFeO*Q* samples was measured from 200 to 900 nm using a PerkinElmer Lambda 650 spectrophotometer. Diffuse-reflectance UV-Visible spectroscopy was used to investigate the magnitude and nature of the band gap of all four phases. After measuring the reflectance *vs.* wavelength, the Kubelka-Munk function[30] was used to analyze the reflectance data. A Tauc plot $[F(R)h\upsilon]^{1/n}$ *vs*. $[h\upsilon]$ (where $h\upsilon$ is the photon energy and *n* a related to the type of transition exponent) was used to determine the optical bandgap.[31]

Photocurrent measurements were performed using an Autolab PGSTAT204 (Metrohm) electrochemical device coupled to an LED module (LED driver kit, Metrohm). The LEDs (450, 470, 505, 530, 590 and 627 nm with low spectral dispersion) were calibrated using a photodiode to determine the density of the luminous flux received by the sample. The photoelectrochemical measurements were performed in a standard three-electrode cell (Magnetic Mount Photo-electrochemical Cell (Redox.me®), including Ag/AgCl and Pt wire as reference electrode and counter electrode, respectively. The cell allows standardized illumination over 1 cm² by the rear face of the working electrode. The working electrode consisted of the photocatalyst powder dispersed in PVDF (polyvinylidene fluoride) binder (in 2:1 ratio), that was later deposited on an ITO/glass substrate (Delta Technologies, Ltd), using the drop casting technique.[32] The electrolyte employed is an aqueous 0.1 M sodium sulfate (Na_2SO_4) solution. Mott-Schottky tests were used to determine flat band potentials.[33, 34] Depending on the slope of $1/C^2$ vs. applied potential, the flat band potential E_{fb} relative to an Ag/AgCl reference electrode, or the reversible hydrogen electrode (RHE) can be estimated: $E_{RHE} = E_{Ag/AgCl} + E^0_{Ag/AgCl} + 0.059.pH$; where $E^0_{Ag/AgCl\,vs.SHE}$ is the potential of the Ag/AgCl reference electrode with respect to the standard hydrogen electrode (SHE) at 195 mV and the pH of the used electrolyte (5.6 for 0.1 M of Na_2SO_4).

The electronic properties of the non-centrosymmetric CaFeOSe oxyselenide were investigated using density functional theory (DFT). Calculations were carried out by employing the projector-augmented-wave (PAW) method[35, 36] encoded in the Vienna *ab initio* simulation package (VASP)[37] and the generalized gradient approximation (GGA) of Perdew, Burke and Ernzerhof (PBE)[38] for the exchange-correlation functionals. To account for the strong electronic correlation associated with the Fe 3*d* states, the GGA plus on-site repulsion U (GGA+ U) method was employed[39] with U_{eff} = 4 eV in an antiferromagnetic configuration.[40] A plane-wave cutoff energy of 550 eV and a threshold of self-consistent-field energy convergence of 10^{-6} eV were used with ƙ-points meshes (13×4×8) in the irreducible Brillouin zone. It converged with residual Hellman-Feynman forces on the atoms smaller than 0.03 eV $Å^{-1}$ and led to a good match with the experimental structure; i.e. within a reasonable error expected for the GGA method. The relaxed structure was used for calculations of the electronic structure and the charge carrier's effective masses. The effmass software was used order to deal with the spin polarized band structure of the CaFeOSe phase.[41]

Results:

Polycrystalline samples of $La_2O_2Fe_2OQ_2$ and CaFeO*Q* (*Q* = S, Se) were prepared and X-ray powder diffraction was used to monitor synthesis reactions. Rietveld analysis (see SI) confirmed successful preparation of the four phases. Only the non-centrosymmetric, polar polymorph ($Cmc2_1$ symmetry) of CaFeSeO was prepared; attempts to prepare the non-polar phase were not successful.

1) Optical measurements

The band gaps of $La_2O_2Fe_2OQ_2$ (*Q* = S, Se) are too small to be measured optically, but reported electrical measurements suggest electronic band gaps of 0.19-0.24 eV.[27] CaFeOS is reported to be an indirect bandgap semiconductor[42] whilst our DFT calculations (see below) indicate that the polar

CaFeSeO has a direct gap. Tauc plots[31] (with n = 2 and n = ½ for CaFeSO and CaFeSeO, respectively) from our diffuse reflectance measurements (after Kubelka-Munk analysis[30]) suggest optical bandgaps of 1.43(1) eV and 2.11(1) eV for CaFeOS and CaFeOSe, respectively (Figure 2). These values are consistent with literature reports (1.16 eV,[42] 1.8 eV,[24] respectively), and are within the energy range of the solar spectrum (1.23 – 3.1 eV).

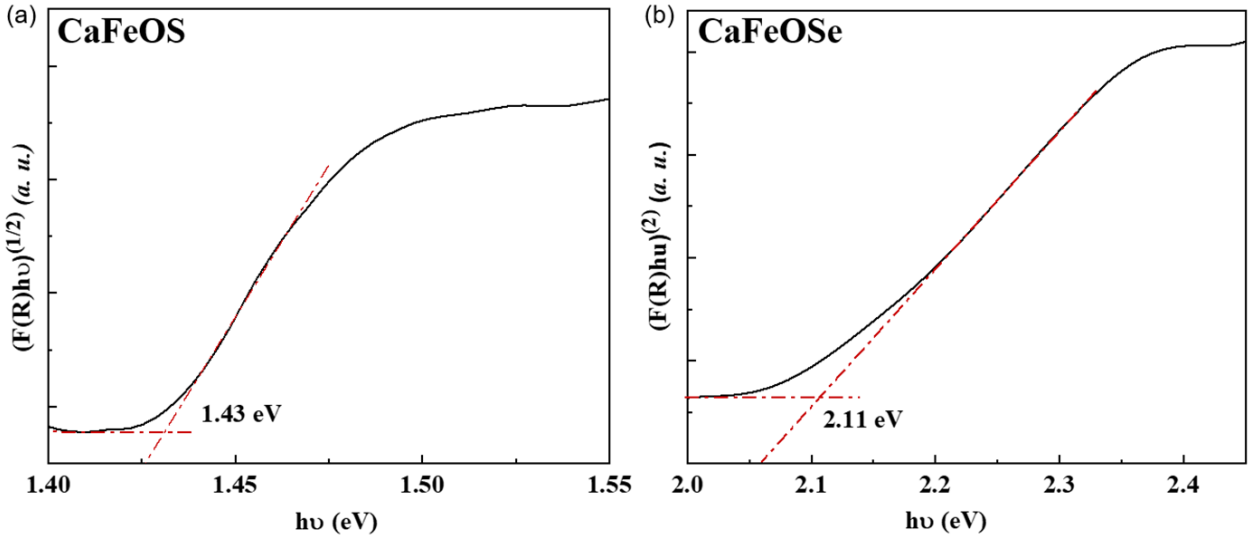

Figure 2 Tauc plots to determine the experimental optical bandgaps for (a) CaFeOS and (b) CaFeOSe.

In addition to the magnitude of the band gap, the band edge positions of photoactive materials must also be consistent with the redox reactions of water. The band edge positions were estimated using an empirical method based on Mullikan electronegativities (see SI) and those for CaFeOQ (Q = S, Se) were found to be compatible with photocathodic water splitting reactions.

2) Mott-Schottky tests

Mott-Schottky tests were performed for CaFeOQ and $La_2O_2Fe_2OQ_2$ (Q = S, Se) at 1 kHz and zero bias voltage to investigate the conduction type, carrier concentration and flat-band potential E_{fb} and plots are shown in Figure 3. The positive slope of $^1/_{C^2}$ with applied potential confirms the n-type nature of these semiconductors. The gradient of the slope can be used to estimate the flat-band potential (close to the CBM)[43] with respect to the reversible hydrogen electrode (RHE) or an Ag/AgCl reference electrode (Table 3). The gradients indicate CBM at -0.205(1) V for CaFeSO and -0.605(1) V for CaFeSeO, and at 0.425(1) V and 0.395(1) V for $La_2O_2Fe_2OQ_2$ (Q = S and Se, respectively). These values are consistent with our empirical calculations (see SI) and suggest the potential of the CaFeOQ materials for solar water splitting reactions.

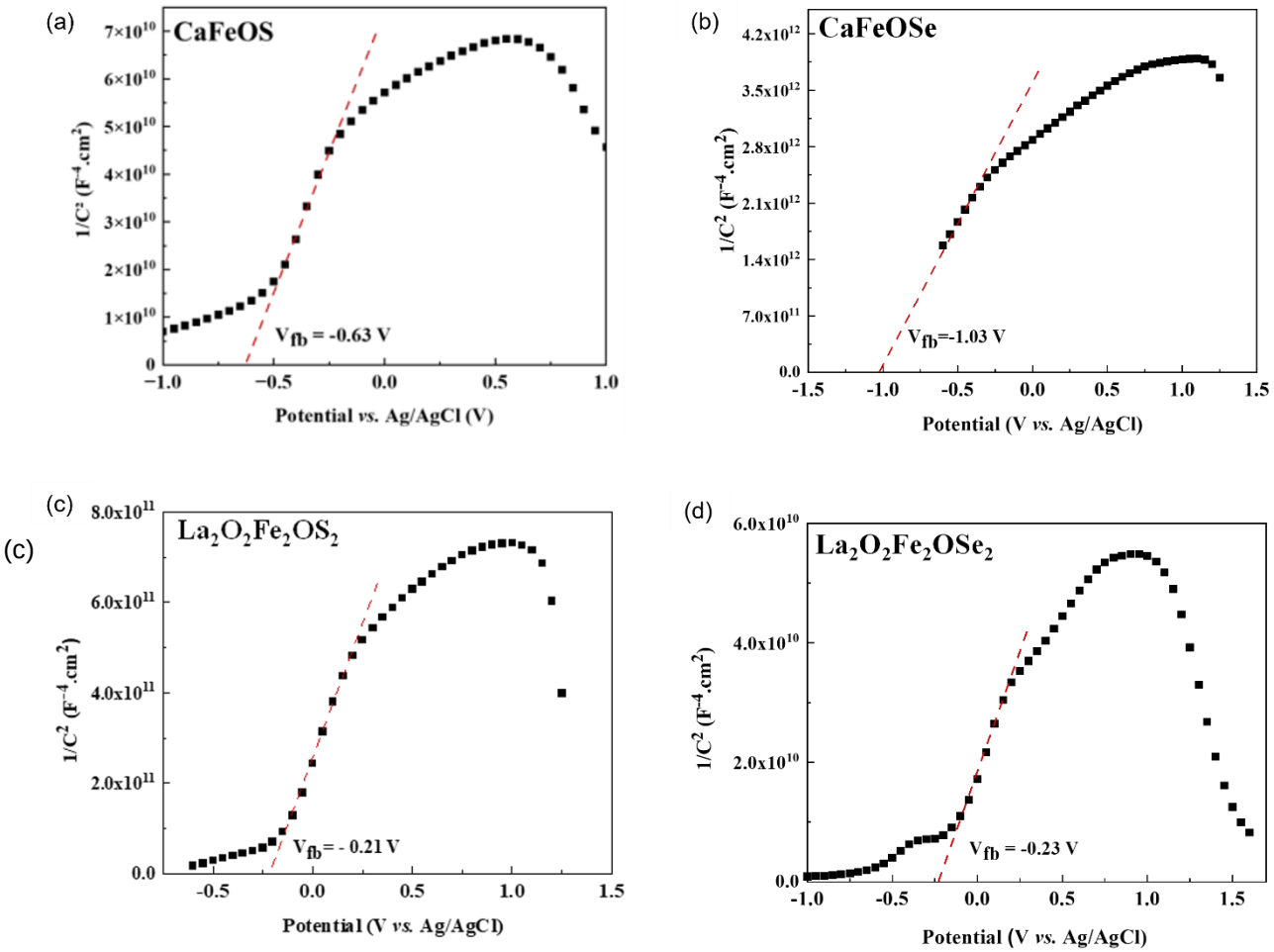

Figure 3 Mott-Schottky plot for (a) CaFeOS, (b) CaFeOSe, (c) $La_2O_2Fe_2OS_2$ and (d) $La_2O_2Fe_2OSe_2$ deposited on ITO/Glass performed at 1 kHz and V_{bias}= 0 V.

Table 1 Conduction band position *vs.* Ag/AgCl and *vs.* RHE

Composition	CB position (V) *vs.*	
	Ag/AgCl	RHE
CaFeOS	-0.63(1)	-0.105(1)
CaFeOSe	-0.75(1)	-0.505(1)
$La_2O_2Fe_2OS_2$	-0.21(1)	0.325(1)
$La_2O_2Fe_2OSe_2$	-0.23(1)	0.295(1)

3) Photocurrent response

The greatest photocurrent response ($\Delta j = j_{illum} - j_{dark}$,where j_{illum} and j_{dark} represent the current density under illumination and darkness) was observed for irradiation with 450 nm light for CaFeSeO, (and with 470 nm light for $La_2O_2Fe_2OQ_2$ (see SI)) and so 450 nm light was used for on/off cycles of 20 s to measure the transient photocurrent responses (Figures 4 and 7).

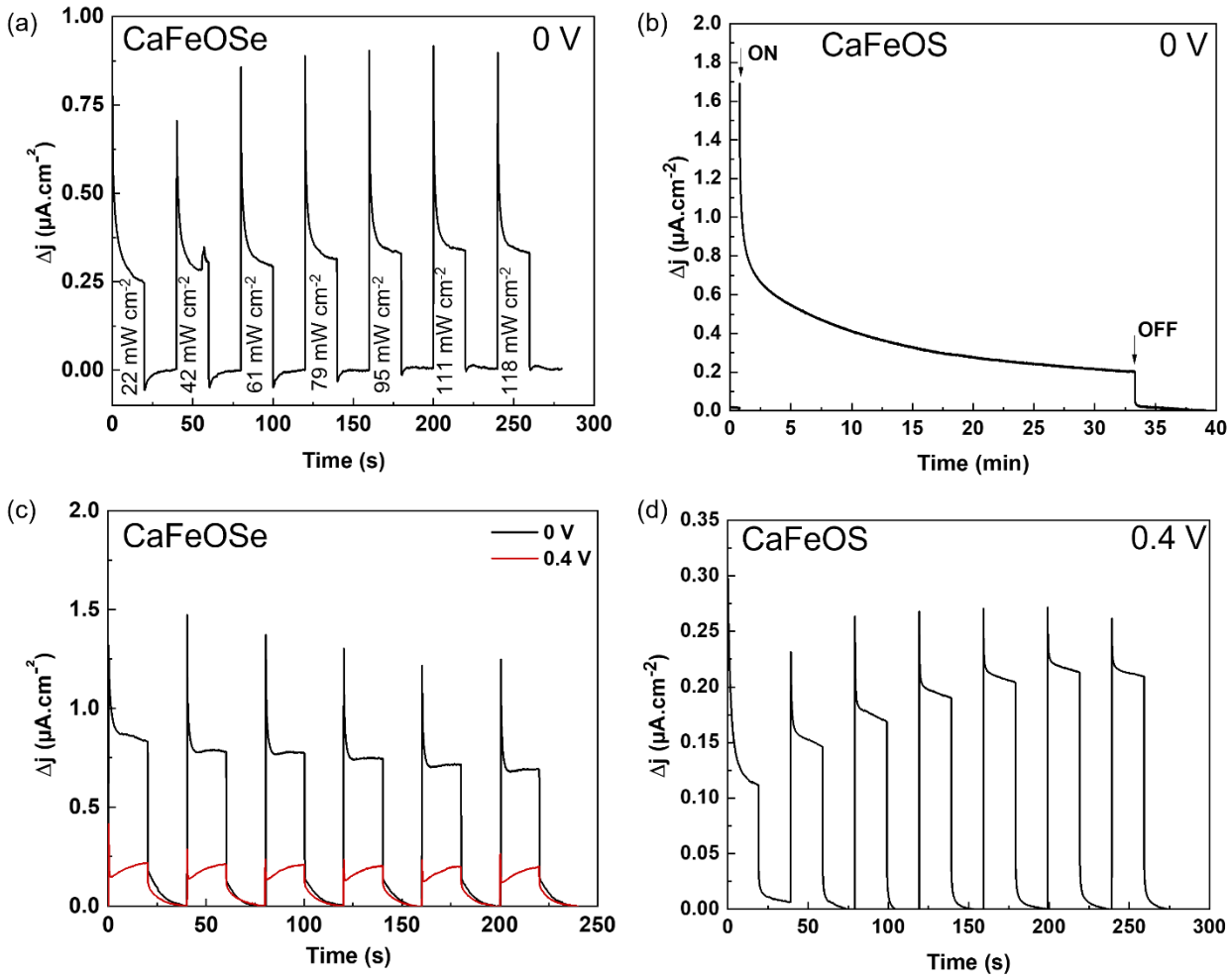

Figure 4 Photocurrent measurements for CaFeSeO: a) shows transient photocurrent response under several light power densities (450 nm excitation) (V_{bias}= 0 V) and (b) shows the variation in current density for CaFeOS (V_{bias} = 0 V) for >30 minutes exposure time to solar light excitation; (c) shows transient photocurrent response under solar illumination (100 mW.cm^{-2}) for V_{bias}= 0 and 0.4 V of CaFeOSe; (d) shows transient photocurrent response under several light power densities (450 nm excitation) for CaFeSeO with V_{bias} = 0.4 V.

CaFeSeO showed a fairly high photocurrent response (up to 0.9 μA cm^{-2} for a power density of 118 mW cm^{-2}) even at $V_{bias} = 0$ V (Figure 4a). The transient photocurrent response shows a spike (charge accumulation at the surface) followed by a decay towards a stable state corresponding to the steady state where the carriers are successfully transferred without undergoing recombination. However, this stable state does not seem to be reached after 20 s of measurement. To verify this, a measurement was carried out over a longer period (Figure 4b) where we observe that this transient state gradually decreases and does not stabilize after 30 minutes. This evolution could indicate slow kinetics in the establishment of the stationary state, with progressive recombination of electron-hole pairs within the material, or a photocorrosion of the electrode (chemical degradation at the interface of the film or progressive dissolution in the electrolyte). The first hypothesis, of slow kinetics, seems more likely because the intensity of the photocurrent remains relatively stable after several ON/OFF cycles under solar irradiation (Figure 4c). Additionally, trap states in the photoconductor can play an important role in extending the lifetime of photogenerated carriers. Thus the long decay may be

due to intrinsic defects (such as impurities, vacancies or interstitial ions) which induce energy levels in the band gap.[44, 45] The recombination phenomena are quite rapid but if the semiconductor contains traps, the establishment of the steady state can be slower with the presence of shallow traps (close to band edges) or even slower with the presence of deep traps (close to middle of band gap).[46] For an applied bias potential of 0.4 V, the behavior evolves with a lower peak height (Figure 4d) indicating a decrease in the recombination rate.

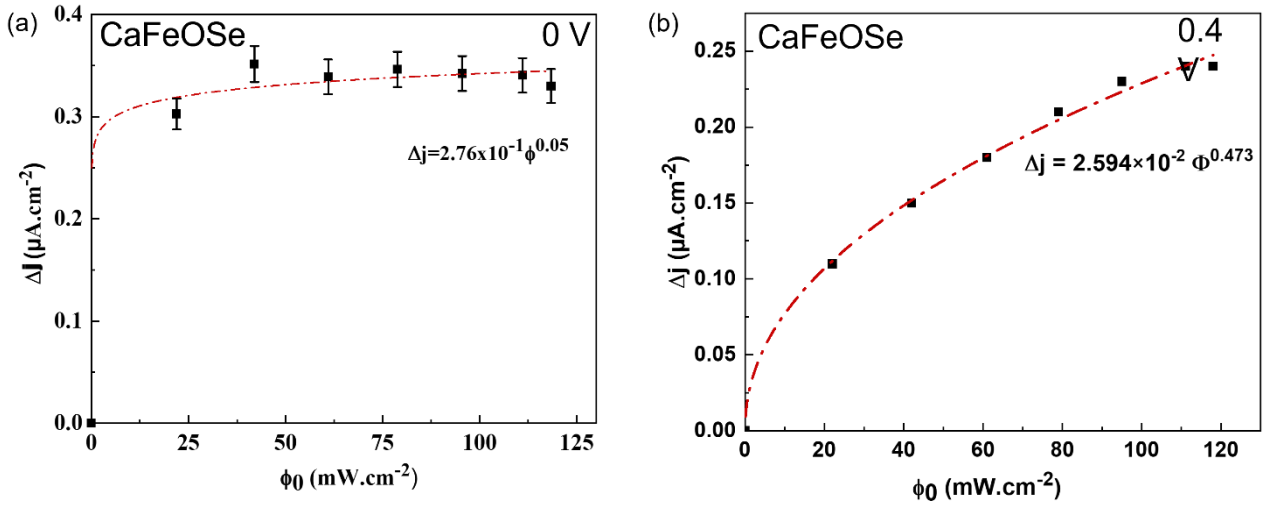

Figure 5 The evolution of the photocurrent density for CaFeOSe with the power density of light under a 450 nm excitation for (a) V_{bias}= 0 V and (b) V_{bias}= 0.4 V.

In addition, the photocurrent response of CaFeSeO was found to increase as a function of the power density of light (Figure 5). This behavior could be fitted by a classical power law.[47] For V_{bias}=0 V, $\Delta j = 2.76\times10^{-1}(2)\Phi^{0.05(2)}$ and the low exponent from this fitting indicates that a saturation regime is quickly reached after 20 s of measurement. Thus, increased illumination power cannot effectively increase the photogain.[48] (The slow recombination kinetics described above are not taken into account in this case because the steady state is not reached.) For V_{bias}=0.4 V, the power law follows a more usual evolution with $\Delta j = 2.59\times10^{-2}(2)\Phi^{0.47(2)}$ indicating faster de-trapping with the application of a bias voltage.

The characteristic shape of the photocurrent response observed for CaFeSeO (Figure 4a) indicates the fast separation of charge carriers (the peak results from the surface being loaded with charge carriers), followed by the system reaching an equilibrium between charge recombination and charge transfer (the decay from the spike to the plateau at steady state).[49] The exponential decrease in the photocurrent from the peak to the plateau can be fitted using a model proposed by Parkinson et al[50] to give values for the transfer and recombination rate constants (Figure 6). For V_{bias} = 0 V, k_{rec} increase monotonically ($k_{rec} = 0.24\ to\ 0.55$ min^{-1} for 21 to 118 mW cm^{-2}) with an increase in ϕ_0 indicating that the recombination of electrons and holes is favored under high light power density (as described for WO_3 photoanodes).[51] The transfer rate remains lower than the recombination rate,

leading to a transfer efficiency of 40%. In contrast, for V_{bias}= 0.4 V the transfer rate is greater than the recombination rate (the recombination rate remains stable at around $k_{rec} = 0.5$ min^{-1}) giving an improvement in transfer efficiency of up to 80% (Figure 6b). These rate constants for $V_{bias} = 0.4$ V calculated for CaFeSeO are noticeably higher than those measured recently for $Sr_6Cd_2Sb_6S_{10}O_7$ ($k_{tr} = 0.25$ min^{-1}; $k_{rec} = 0.08$ min^{-1}).[6] The application of a potential therefore promotes the transfer of charge at the interface.

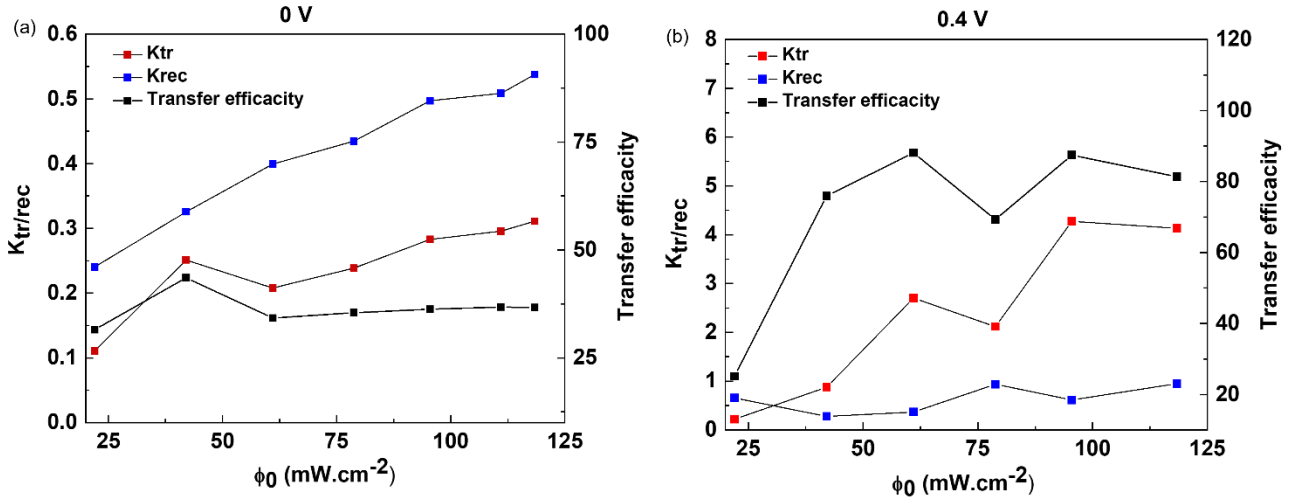

Figure 6 Evolution of the recombination and transfer rate constants k_{tr} and k_{rec} with intensity of light alongside the transfer efficacy η_k by intensity light of CaFeOSe at (a) 0 V and (b) 0.4 V.

The transient photocurrent response of CaFeSeO under solar illumination (simulated using a 150 W xenon lamp with AM 1.5G filter, 100 mW cm^{-2}) was also measured for $V_{bias} = 0$ and 0.4 V for on/off cycles of 20 s (Figure 4(c)). Apart from the good reproducibility of the measurements over the different cycles, two behaviors are observed. Firstly, for $V_{bias} = 0$ V with high photocurrents (1.45 μA cm^{-2}), the steady state is not reached within the measurement time. Secondly, for $V_{bias} = 0.4$ V, a more stable but lower photocurrent (0.35 μA cm^{-2}) is measured.

For CaFeSO, no photocurrent response was detected for $V_{bias} = 0.0$ V. It is necessary to apply a voltage of 0.6 V in order to observe less stable and much weaker photocurrents (~40 nA cm^{-2} for a power density of 111 mW cm^{-2} (450 nm), see SI) compared with the oxyselenide analogue, demonstrating poor performance of this material. Furthermore, for higher potentials the response is erratic until it completely disappears, indicating strong photocorrosion of the film. This could result from some degradation of the CaFeSO film, particularly under the higher bias voltage of $V_{bias} = 0.6$ V. Linear sweep measurements (see SI) give evidence of an oxidation reaction for the sample-electrolyte system; likely indicating that some oxidation of Fe^{2+} in the sample occurs.

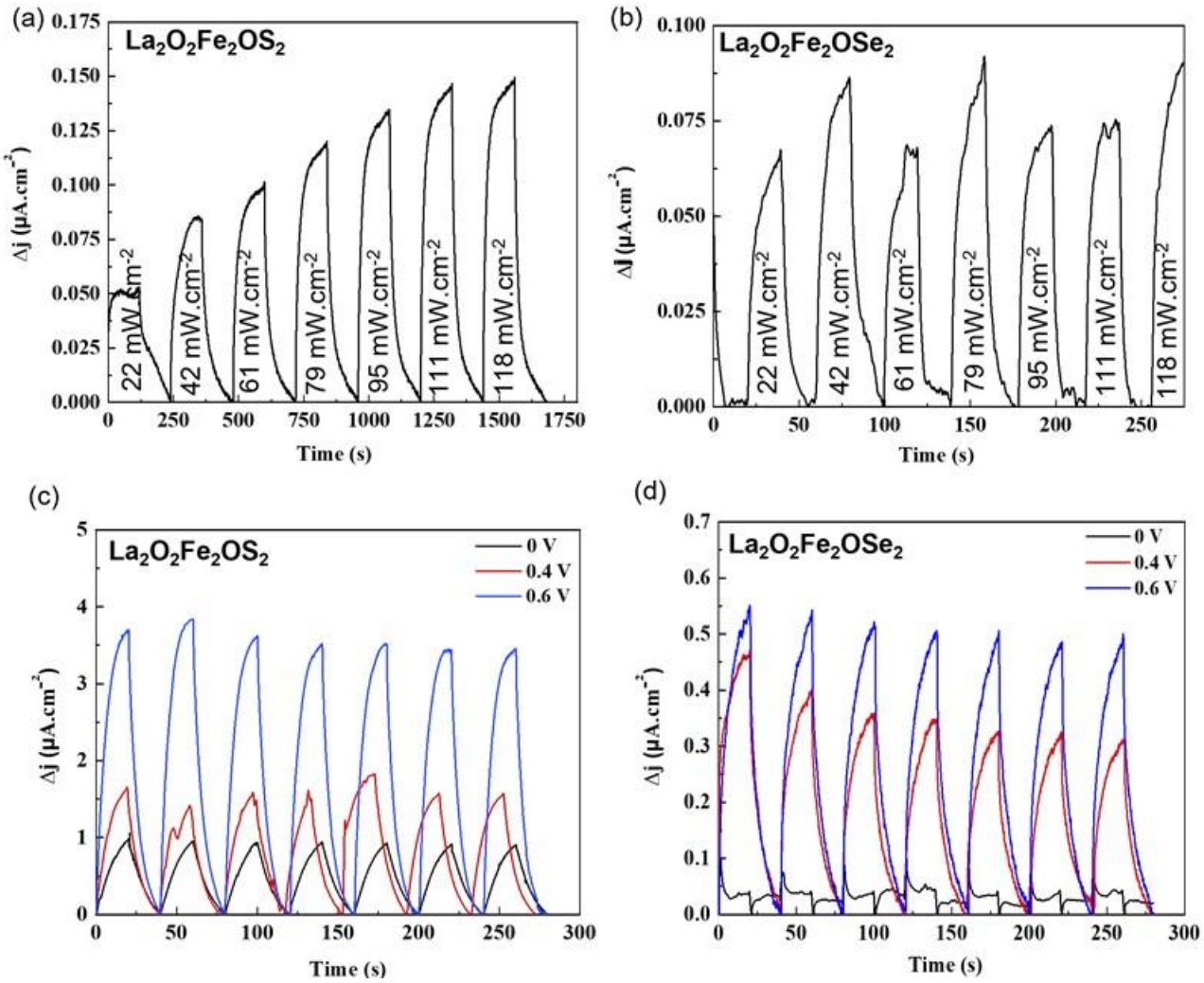

Figure 7 Transient photocurrent response under a 450 nm excitation of (a) $La_2O_2Fe_2OS_2$, (b) $La_2O_2Fe_2OSe_2$; and under solar illumination (100 mW.cm^{-2}) for V_{bias}= 0, 0.4 and 0.6 V of (c) $La_2O_2Fe_2OS_2$, (d) $La_2O_2Fe_2OSe_2$.

Similar photocurrent response measurements for $La_2O_2Fe_2OQ_2$ showed a stable photocurrent (up to 0.15 μA cm^{-2}) for Q = S (Figure 7a), and the study of the transient photocurrent response over a longer time (see SI) shows good stability with only a very slight decrease over >30 minutes. An unstable and lower (up to 0.08 μA cm^{-2}) photocurrent was measured for Q = Se (Figure 7b). The transient current has slower kinetics for the oxyselenide phase, demonstrated by the faster exponential growth for the oxysulfide (Figures 7c and 7d). The transient photocurrent responses were also measured for $La_2O_2Fe_2OQ_2$ under solar illumination (simulated using a 150 W xenon lamp with AM 1.5G filter, 100 mW cm^{-2}) for $V_{bias} = 0, 0.4, 0.6$ V (Figure 7(c), (d)). As expected, the measured photocurrent increased with increasing V_{bias}, although a slight decrease in photocurrent with time was observed under applied voltage, possibly indicating some photocorrosion (chemical degradation or dissolution of the electrode in the electrolyte) which seems to be more significant for $La_2O_2Fe_2OSe_2$. The evolution of the photocurrent response with power density was also measured for $La_2O_2Fe_2OS_2$ (see SI) and showed behaviour consistent with a much high exponent (0.60(2)) than that determined for CaFeOSe (Figure 4d) indicating for fewer traps for $La_2O_2Fe_2OS_2$ than for

the other oxychalcogenides discussed here. This evolution of the photocurrent according to the luminous flux indicates the potential of $La_2O_2Fe_2OS_2$ for photodetector applications.

4) Electronic structure

The band structure and projected density of states (PDOS) were calculated for the polar polymorph of CaFeOSe studied here (Figure 8), for comparison with the electronic structures reported for CaFeOS and for $La_2O_2Fe_2OQ_2$.[27] Our calculations suggest a direct band gap of 2.08 eV for the polar polymorph of CaFeOSe (consistent with our optical measurements, Figure 2), in contrast to the indirect nature reported for the non-polar polymorph.[24] The Fe 3d states dominate the bottom of the conduction band, and also hybridize with the O 2p and Se 3p states to form the top of the valence band (Figure 8b). This is comparable with the PDOS reported for the non-polar polymorph of CaFeOSe,[24] and qualitatively similar to that reported for CaFeOS.[23] Analysis of the fat band plots of the Fe orbitals (spin up and down) in Figure 8c indicates a high spin state.

The band dispersions can give insight into the carrier mobilities. Different dispersions at the CBM and VBM suggest different mobilities of electrons and holes. The lowest electron effective mass $m_e^* = 0.342(3)\ m_0$ was found for the electrons in the conduction band for the $\Gamma \rightarrow S$ direction (i.e. within the layers), whilst the hole effective mass was heavier ($m_h^* = 3.616(3)\ m_0$) along this direction. This indicates a high intralayer mobility for the electrons ($m_e^* < 0.5\ m_0$) and lower mobility for the holes. This is consistent with computational work suggesting that having s orbital character at the CBM (see the Fe 4s contribution to the spin-up channel, Figure 8c) can give low effective masses.[52]

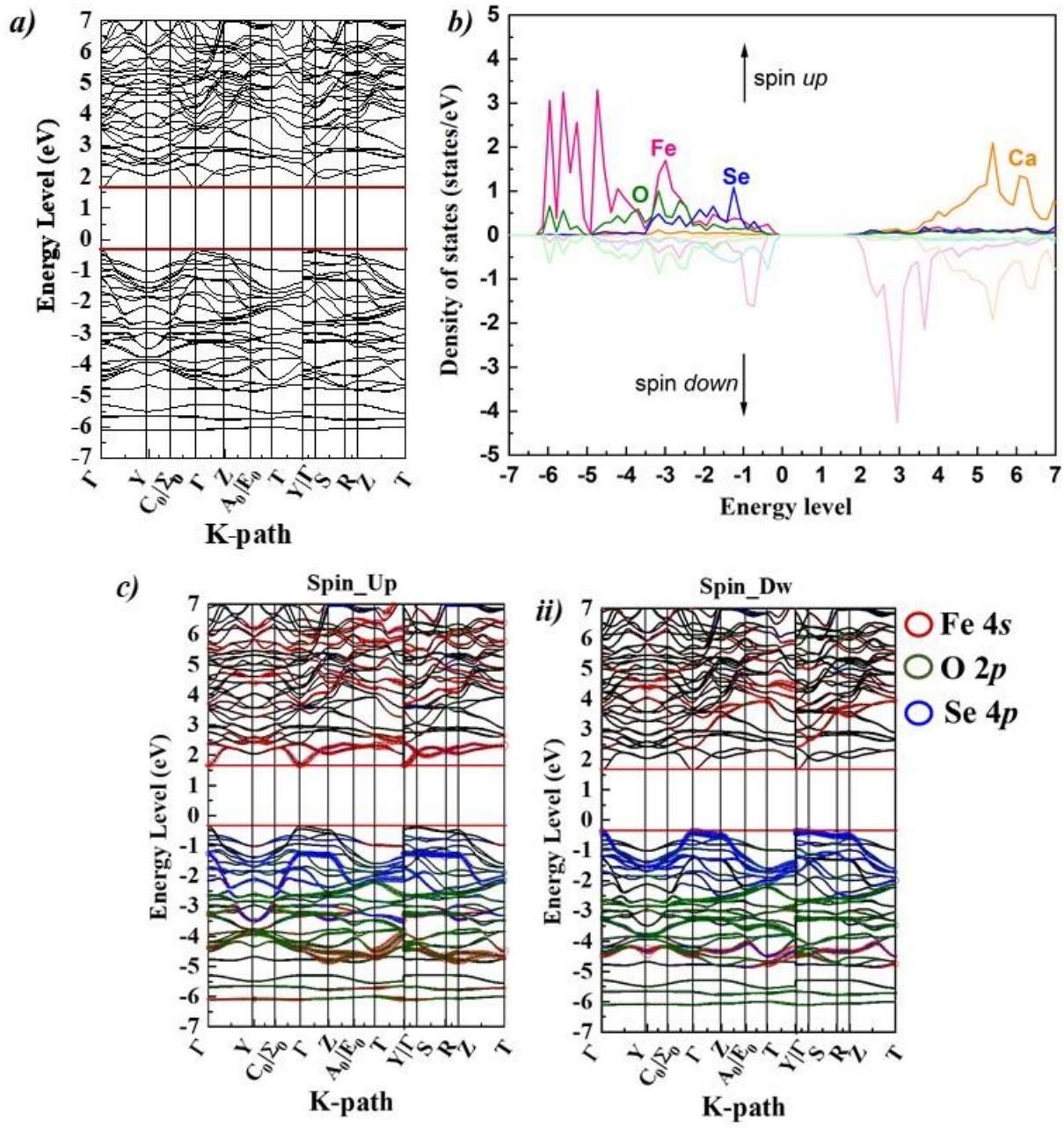

Figure 8 DFT calculations of the non-centrosymmetric (*Cmc*2$_1$) polymorph of CaFeOSe with (a) Electronic band structure, (b) projected density of states (PDOS) and (c) fat bands showing the Fe 3*d* states in (i) spin up and (ii) spin down.

Discussion:

The iron oxychalcogenides investigated here share common features, including their layered crystal structures (Figure 1) and the mixed-anion coordination environments of Fe^{2+} cations (FeO_2Q_4 for $La_2O_2Fe_2OQ_2$, $FeOS_3$ for CaFeOS and $FeSe_2O_2$ for CaFeOSe). These features allow us to explore structure – property relationships in the context of photocatalysis for this family of materials.

Both CaFeSeO and CaFeSO have band gaps well-matched to the solar spectrum (1.43 eV and 2.11 eV for *Q* = S and Se, respectively, Figure 2). This contrasts with the Fe^{2+} oxide $CaFeO_2$ (composed of puckered FeO_4 square planar units) with a much larger band gap ~ 2.7 eV.[53-55] DFT studies on CaFeO*Q* (*Q* = S, Se) suggest that the VBM and CBM are predominantly composed of Fe 3d states

but with significant hybridisation with *Q* *n*p states,[23, 24] presumably contributing to the wider bands and the reduced band gap in these oxychalcogenides. The reduction in bandgap for CaFeOS compared with CaFeOSe is likely due to the increased ratio of chalcogenide to oxide in the pseudo-tetrahedral Fe coordination environment (FeS_3O units in the oxysulfide compared with $FeSe_2O_2$ units in the oxyselenide),[56] and the effect of chemical pressure with the smaller sulfide anion.[57] The much smaller bandgaps for $La_2O_2Fe_2OQ_2$ reflects the different Fe environments and connectivity in these Mott insulators: the 180° Fe – O – Fe bond angles (Figure 9) give better orbital overlap and more dispersed bands, contributing to the small band gaps in these materials.[27] This contrasts with CaFeO*Q* phases with 113° Fe – O – Fe and 104° Fe – S – Fe bond angles connecting Fe-centred tetrahedra for *Q* = Se and S, respectively, giving flatter bands and wider band gaps (Figure 8 and [23]).

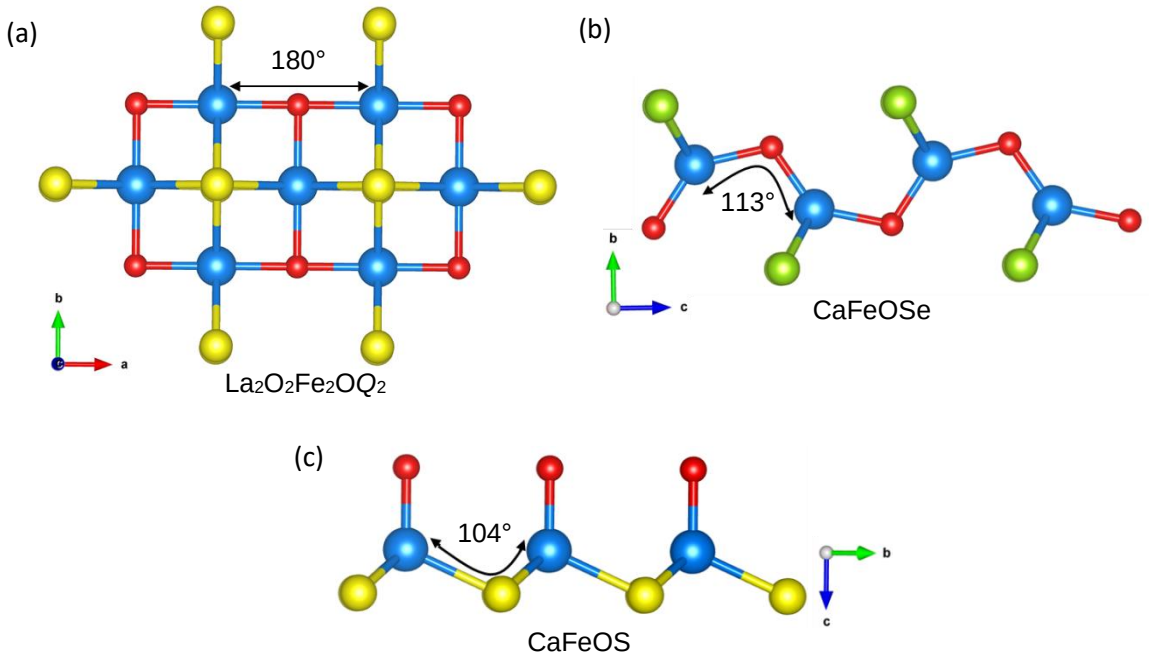

Figure 9 Representation of the M-O/*Q*-M bond angles in (a) $La_2O_2Fe_2OQ_2$ (*Q* = S, Se), (b) CaFeOSe and (c) CaFeOS.

Both $La_2O_2Fe_2OQ_2$ and CaFeO*Q* (*Q* = S, Se) phases generated reproducible photocurrents under solar irradiation and in the whole visible spectrum range. The spike observed in transient photocurrent response for CaFeSeO indicates fast carrier generation (e^- – h^+ separation), then the establishment of a steady state with a balance between transfer and recombination phenomena, notably at the surface of the sample (Figure 4). It has been shown that an internal field due to a polar crystal structure (e.g. in ferroelectrics) minimises charge carrier recombination and instead favours transfer at the interfaces.[58] Both CaFeSeO and CaFeSO samples studied in this work adopt polar crystal structures (of $Cmc2_1$ and $P6_3mc$ symmetries, respectively),[18, 25] and are composed of polar units (FeO_2Se_2 and $FeOS_3$ pseudo-tetrahedra), in contrast to the centrosymmetric, non-polar structures of $La_2O_2Fe_2OQ_2$ ($I4/mmm$ symmetry) with slower kinetics. It's not clear whether a dipole

across the photo-active cation, or a polar axis in the crystal structure, would have the greater effect enhancing e^- – h^+ separation. Comparison with $LaGaS_2O$ (with a non-polar structure of $Pbcm$ symmetry, but composed of polar GaO_2S_2 units)[59] which shows a qualitatively similar photocurrent response with fast e^- – h^+ separation[60] suggests that the local polarity of the photoactive units might be more significant than the overall polarity of the crystal structure. Similar studies on the non-polar polymorph of CaFeSeO[24] would be interesting to confirm this. It is interesting that a higher photocurrent was observed for CaFeOSe with $V_{bias} = 0.0$ V (1.45 μA cm^{-2}) compared with $V_{bias} = 0.4$ V (0.35 μA cm^{-2}). This could be explained by some film degradation in applied voltage. Further investigations are needed to understand this behaviour.

The very different photochemical behaviour of CaFeOSe and CaFeOS (Figure 4 and SI) results from the oxidative degradation of CaFeOS (at $V_{bias} = 0.6$ V). This illustrates that stability of the photoactive oxychalcogenide is an important challenge to overcome in developing this family of materials. Lower oxidation states and coordination numbers can often be stabilised in oxychalcogenides compared with typical oxides,[61] but this can leave the transition metal susceptible to oxidation, depending on the conditions. The greater stability of CaFeOSe here might be due to the greater concentration of electronegative oxide ions in the FeO_2Se_2 units stabilising the Fe^{2+} cation, compared with the $FeOS_3$ units in CaFeOS. It has been reported that holes in d bands of transition metal dichalcogenides might react quite differently to holes in p bands of p block chalcogenides,[62] suggesting that further research might be needed to understand the different stabilities of p block vs transition metal oxychalcogenides in conditions for photoelectrochemical reactions. Related to this, the surface morphology of these samples could also play a key role in their performance and stability. Surface states (associated with dangling bonds at surfaces exposed to the electrolyte) can be detrimental to performance, acting as charge recombination centres,[63] or conversely under appropriate irradiation can act as electron donors giving a photocurrent response.[64] Studies on the surface morphology and modification (as carried out ferrites)[65, 66] would be useful to optimise the stability and performance of CaFeOSe.

Conclusions:

The structural and physical properties of four iron-based oxychalcogenides $La_2O_2Fe_2OQ_2$ and CaFeO*Q* (*Q* = S, Se) were investigated by exploring their photoelectrochemical and electronic characteristics to determine their potential as photocatalysts. The optical band gaps of CaFeO*Q* (E_g = 1.43 and 2.11 eV for *Q* = S and Se, respectively) and conduction band edge positions were found to be suitable for half reactions in visible light as photocathodes. The band gaps of Mott insulating $La_2O_2Fe_2OQ_2$ (*Q* = S, Se) were too small for photocatalytic activity. The transient photocurrent response of CaFeOSe shows spikes (Figure 4), indicating very efficient electron-hole separation and migration, consistent with effective masses calculated by DFT. The O:*Q* ratio in the Fe^{2+} coordination environment in CaFeOSe to give O-linked FeO_2Se_2 tetrahedra seems to reflect a balance between

stabilizing the Fe^{2+} cation (in contrast to CaFeOS which was oxidized by the electrolyte) and reducing the band gap to match the visible spectrum. Further work to investigate the role of mixed-anion environments in tuning band gap, stability, and polarity of coordination environments, and the balance between these for optimal performance, would give important insights for designing new photoactive materials including photocatalysts with activity under solar irradiation.

Supporting Information. The supporting Information is available free of charge.

Rietveld refinement details of $La_2O_2Fe_2OQ_2$ and CaFeO*Q* (*Q* = S, Se) using room temperature XRPD data; Additional experimental details related to the band edges positions and electrochemical additional measurements (PDF).

Acknowledgements:
The I-Site (ULNE), University of Lille, and University of Kent are thanked for Cotutelle funding (S.A.B.). Durham University is thanked for hosting research visit. Dr. Donna Arnold is thanked for helpful discussions. This study was supported by the French government through the Programme Investissement d'Avenir (I-SITE ULNE/ANR-16-IDEX-0004 ULNE)managed by the Agence Nationale de la Recherche (Project ANION-COMBO). X-ray diffractometers are funded by Region NPDC, FEDER, CNRS, and MESR. The regional computational cluster supported by Lille University, CPER Nord-Pas-de Calais/CRDER, France Grille CNRS, and FEDER is thanked for providing computational resources. DIM 1: "energy efficiency" of UArtois is thanked for its help in photocurrent measurements.

References:

1. Kong, D.; Zheng, Y.; Kobielusz, M.; Wang, Y.; Bai, Z.; Macyk, W.; Wang, X.; Tang, J., Recent advances in visible light-driven water oxidation and reduction in suspension systems. *Materials Today* **2018,** *21* (8), 897-924.
2. Hashimoto, K.; Irie, H.; Fujishima, A., TiO2 Photocatalysis: A Historical Overview and Future Prospects. *Japanese Journal of Applied Physics* **2005,** *44* (12R), 8269.
3. Maruska, H. P.; Ghosh, A. K., Photocatalytic decomposition of water at semiconductor electrodes. *Solar Energy* **1978,** *20* (6), 443-458.
4. Scheer, R.; Walter, T.; Schock, H. W.; Fearheiley, M. L.; Lewerenz, H. J., CuInS2 based thin film solar cell with 10.2% efficiency. *Applied Physics Letters* **1993,** *63* (24), 3294-3296.
5. Maeda, K.; Domen, K., New Non-Oxide Photocatalysts Designed for Overall Water Splitting under Visible Light. *The Journal of Physical Chemistry C* **2007,** *111* (22), 7851-7861.
6. Bacha, S. A.; Saitzek, S.; McCabe, E. E.; Kabbour, H., Photocatalytic and photoconduction response under visible light of the lone pair based oxysulfide Sr6Cd2Sb6O7S10. *Inorg. Chem.* **2022,** *61*, 18611-18621.
7. Wang, R.; Wang, F.; Zhang, X.; Feng, X.; Zhao, C.; Bu, K.; Zhang, Z.; Zhai, T.; Huang, F., Improved Polarization in the Sr6Cd2Sb6O7Se10 Oxyselenide through Design of Lateral Sublattices for Efficient Photoelectric Conversion. *Angewandte Chemie International Edition* **2022,** *61* (33), e202206816.
8. Miura, A.; Oshima, T.; Maeda, K.; Mizuguchi, Y.; Moriyoshi, C.; Kuroiwa, Y.; Meng, Y.; Wen, X.-D.; Nagao, M.; Higuchi, M.; Tadanaga, K., Synthesis, structure and photocatalytic activity of layered LaOInS2. *Journal of Materials Chemistry A* **2017,** *5* (27), 14270-14277.
9. Kabbour, H.; Sayede, A.; Saitzek, S.; Lefevre, G.; Cario, L.; Trentesaux, M.; Roussel, P., Structure of the water-splitting photocatalyst oxysulfide alpha-LaOInS2 and ab initio prediction of new polymorphs. *Chemical Communications* **2020,** *56* (11), 1645-1648.
10. Ishikawa, A.; Takata, T.; Kondo, J. N.; Hara, M.; Kobayashi, H.; Domen, K., Oxysulfide Sm2Ti2S2O5 as a stable photocatalyst for water oxidation and reduction under visible light irradiation (lambda <= 650 nm). *Journal of the American Chemical Society* **2002,** *124* (45), 13547-13553.
11. Wang, Q.; Nakabayashi, M.; Hisatomi, T.; Sun, S.; Akiyama, S.; Wang, Z.; Pan, Z.; Xiao, X.; Watanabe, T.; Yamada, T.; Shibata, N.; Takata, T.; Domen, K., Oxysulfide photocatalyst for visible-light-driven overall water splitting. *Nature Materials* **2019,** *18* (8), 827-832.
12. Tiwari, R. P., Visible-Light-Activated Enhanced Shift Current Bulk Photovoltaic Effect in Lead-Free Oxychalcogenide Perovskites: Emergence of Fully Inorganic Photovoltaic Materials. *The Journal of Physical Chemistry C* **2022,** *126* (25), 10258-10265.

13. Park, H.; Alharbi, F. H.; Sanvito, S.; Tabet, N.; El-Mellouhi, F., Searching for Photoactive Polymorphs of CsNbQ3 (Q = O, S, Se, Te) with Enhanced Optical Properties and Intrinsic Thermodynamic Stabilities. *The Journal of Physical Chemistry C* **2018,** *122* (16), 8814-8821.
14. Park, H.; Alharbi, F. H.; Sanvito, S.; Tabet, N.; El-Mellouhi, F., Elucidating the Impact of Chalcogen Content on the Photovoltaic Properties of Oxychalcogenide Perovkskites: NaMO3−xQx (M=Nb, Ta; Q=S, Se, Te). *ChemPhysChem* **2018,** *19* (6), 703-714.
15. Dong, X.-D.; Zhang, Y.-M.; Zhao, Z.-Y., Role of the Polar Electric Field in Bismuth Oxyhalides for Photocatalytic Water Splitting. *Inorganic Chemistry* **2021,** *60* (12), 8461-8474.
16. Lou, Z.; Wang, P.; Huang, B.; Dai, Y.; Qin, X.; Zhang, X.; Wang, Z.; Liu, Y., Enhancing Charge Separation in Photocatalysts with Internal Polar Electric Fields. *ChemPhotoChem* **2017,** *1* (5), 136-147.
17. Vonrüti, N.; Aschauer, U., Band-gap engineering in AB(OxS1−x)3 perovskite oxysulfides: a route to strongly polar materials for photocatalytic water splitting. *Journal of Materials Chemistry A* **2019,** *7* (26), 15741-15748.
18. Jin, S. F.; Huang, Q.; Lin, Z. P.; Li, Z. L.; Wu, X. Z.; Ying, T. P.; Wang, G.; Chen, X. L., Two-dimensional magnetic correlations and partial long-range order in geometrically frustrated CaOFeS with triangle lattice of Fe ions. *Phys. Rev. B* **2015,** *91* (9), 094420.
19. Delacotte, C.; Pérez, O.; Pautrat, A.; Berthebaud, D.; Hébert, S.; Suard, E.; Pelloquin, D.; Maignan, A., Magnetodielectric Effect in Crystals of the Noncentrosymmetric CaOFeS at Low Temperature. *Inorganic Chemistry* **2015,** *54* (13), 6560-6565.
20. Selivanov, E. N.; Chumarev, V. M.; Gulyaeva, R. I.; Mar'evich, V. P.; Vershinin, A. D.; Pankratov, A. A.; Korepanova, E. S., Composition, Structure, and Thermal Expansion of Ca3Fe4S3O6 and CaFeSO. *Inorganic Materials* **2004,** *40* (8), 845-850.
21. Sambrook, T.; Smura, C. F.; Clarke, S. J.; Ok, K. M.; Halasyamani, P. S., Structure and Physical Properties of the Polar Oxysulfide CaZnOS. *Inorganic Chemistry* **2007,** *46* (7), 2571-2574.
22. Petrova, S. A.; Mar'evich, V. P.; Zakharov, R. G.; Selivanov, E. N.; Chumarev, V. M.; Udoeva, L. Y., Crystal Structure of Zinc Calcium Oxysulfide. *Doklady Chemistry* **2003,** *393* (1), 255-258.
23. Zhang, Y.; Lin, L.; Zhang, J.-J.; Huang, X.; An, M.; Dong, S., Exchange striction driven magnetodielectric effect and potential photovoltaic effect in polar CaOFeS. *Physical Review Materials* **2017,** *1* (3), 034406.
24. Han, F.; Wang, D.; Malliakas, C. D.; Sturza, M.; Chung, D. Y.; Wan, X.; Kanatzidis, M. G., (CaO)(FeSe): A Layered Wide-Gap Oxychalcogenide Semiconductor. *Chem. Mater.* **2015,** *27* (16), 5695-5701.
25. Cassidy, S. J.; Batuk, M.; Batuk, D.; Hadermann, J.; Woodruff, D. N.; Thompson, A. L.; Clarke, S. J., Complex Microstructure and Magnetism in Polymorphic CaFeSeO. *Inorg. Chem.* **2016,** *55* (20), 10714-10726.
26. Mayer, J. M.; Schneemeyer, L. F.; Siegrist, T.; Waszczak, J. V.; Van Dover, B., New Layered Iron-Lanthanum-Oxide-Sulfide and -Selenide Phases: Fe2La2O3E2(E = S,Se). *Angew. Chem. Int. Ed.* **1992,** *31* (12), 1645-1647.
27. Zhu, J.-X.; Yu, R.; Wang, H.; Zhao, L. L.; Jones, M. D.; Dai, J.; Abrahams, E.; Morosan, E.; Fang, M.; Si, Q., Band Narrowing and Mott Localization in Iron Oxychalcogenides La2O2Fe2O(S, Se)2. *Phys. Rev. Lett.* **2010,** *104* (21), 216405.
28. Rodriguez-Carvajal, J. *A Program for Rietveld Refinement and Profile Matching Analysis of Complex Powder Diffraction Patterns*, Laboratoire Léon Brillouin (CEA-CNRS), 1991.
29. Momma, K.; Izumi, F., VESTA 3 for three-dimensional visualization of crystal, volumetric and morphology data. *J. Appl. Cryst.* **2011,** *44*, 1272-1276.
30. Kubelka, P.; Munk, F., Ein Beitrag zur Optik der Farbanstriche. *Z. Techn. Phys.* **1931,** *12*, 593-601.
31. Tauc, J.; Grigorovici, R.; Vancu, A., Optical Properties and Electronic Structure of Amorphous Germanium. *physica status solidi (b)* **1966,** *15* (2), 627-637.
32. Mentré, O.; Juárez-Rosete, M. A.; Saitzek, S.; Aguilar-Maldonado, C.; Colmont, M.; Arévalo-López, Á. M., S = 1/2 Chain in BiVO3F: Spin Dimers versus Photoanodic Properties. *Journal of the American Chemical Society* **2021,** *143* (18), 6942-6951.
33. Leroy, S.; Blach, J.-F.; Huvé, M.; Léger, B.; Kania, N.; Henninot, J.-F.; Ponchel, A.; Saitzek, S., Photocatalytic and sonophotocatalytic degradation of rhodamine B by nano-sized La2Ti2O7 oxides synthesized with sol-gel method. *Journal of Photochemistry and Photobiology A: Chemistry* **2020,** *401*, 112767.
34. Gelderman, K.; Lee, L.; Donne, S. W., Flat-Band Potential of a Semiconductor: Using the Mott–Schottky Equation. *Journal of Chemical Education* **2007,** *84* (4), 685.
35. Kresse, G.; Joubert, D., From ultrasoft pseudopotentials to the projector augmented-wave method. *Physical Review B* **1999,** *59* (3), 1758-1775.
36. Blöchl, P. E., Projector augmented-wave method. *Physical Review B* **1994,** *50* (24), 17953-17979.

37. Sun, G.; Kürti, J.; Rajczy, P.; Kertesz, M.; Hafner, J.; Kresse, G., Performance of the Vienna ab initio simulation package (VASP) in chemical applications. *Journal of Molecular Structure: THEOCHEM* **2003,** *624* (1), 37-45.
38. Perdew, J. P.; Burke, K.; Ernzerhof, M., Generalized Gradient Approximation Made Simple. *Physical Review Letters* **1996,** *77* (18), 3865-3868.
39. Dudarev, S. L.; Botton, G. A.; Savrasov, S. Y.; Humphreys, C. J.; Sutton, A. P., Electron-energy-loss spectra and the structural stability of nickel oxide: An LSDA+U study. *Physical Review B* **1998,** *57* (3), 1505-1509.
40. Lai, K. T.; Komarek, A. C.; Fernández-Díaz, M. T.; Chang, P.-S.; Huh, S.; Rosner, H.; Kuo, C.-Y.; Hu, Z.; Pi, T.-W.; Adler, P.; Ksenofontov, V.; Tjeng, L. H.; Valldor, M., Canted Antiferromagnetism on Rectangular Layers of Fe2+ in Polymorphic CaFeSeO. *Inorg. Chem.* **2017,** *56* (8), 4271-4279.
41. Whalley, L. D., effmass: an effective mass package. *J. Open Source Software* **2018,** *3*, 797.
42. Zhang, Y.; Lin, L.; Zhang, J.-J.; Huang, X.; An, M.; Dong, S., Exchange striction driven magnetodielectric effect and potential photovoltaic effect in polar CaOFeS. *Phys. Rev. Materials* **2017,** *1*, 034406.
43. Lin, L.; Lin, J. M.; Wu, J. H.; Hao, S. C.; Lan, Z., Photovoltage enhancement of dye sensitised solar cells by using ZnO modified TiO2 electrode. *Materials Research Innovations* **2010,** *14* (5), 370-374.
44. Hou, Y.; Mei, Z.; Du, X., Semiconductor ultraviolet photodetectors based on ZnO and MgxZn1−xO. *Journal of Physics D: Applied Physics* **2014,** *47* (28), 283001.
45. Murphy, T. E.; Moazzami, K.; Phillips, J. D., Trap-related photoconductivity in ZnO epilayers. *Journal of Electronic Materials* **2006,** *35* (4), 543-549.
46. Jiang, J.; Ling, C.; Xu, T.; Wang, W.; Niu, X.; Zafar, A.; Yan, Z.; Wang, X.; You, Y.; Sun, L.; Lu, J.; Wang, J.; Ni, Z., Defect Engineering for Modulating the Trap States in 2D Photoconductors. *Advanced Materials* **2018,** *30* (40), 1804332.
47. Shaikh, S. K.; Inamdar, S. I.; Ganbavle, V. V.; Rajpure, K. Y., Chemical bath deposited ZnO thin film based UV photoconductive detector. *Journal of Alloys and Compounds* **2016,** *664*, 242-249.
48. Zhao, Q.; Wang, W.; Carrascoso-Plana, F.; Jie, W.; Wang, T.; Castellanos-Gomez, A.; Frisenda, R., The role of traps in the photocurrent generation mechanism in thin InSe photodetectors. *Materials Horizons* **2020,** *7* (1), 252-262.
49. Leroy, S. Etude des propriétés photocatalytiques et photoélectriques du dititanate de lanthane (La2Ti2O7) à structure pérovskite en feuillets et son utilisation dans des hétérojonctions tout oxyde pour la conversion d'énergie. Universite d'Artois, 2020.
50. Parkinson, B.; Turner, J.; Peter, L.; Lewis, N.; Sivula, K.; Domen, K.; Bard, A. J.; Fiechter, S.; Collazo, R.; Hannappel, T., The Potential Contribution of Photoelectrochemistry in the Global Energy Future. In *Photoelectrochemical Water Splitting Materials, Processes and Architectures*, Lewerenze, H.-J.; Peter, L., Eds. RSC: 2013; Vol. 9.
51. Amano, F.; Koga, S., Influence of light intensity on the steady-state kinetics in tungsten trioxide particulate photoanode studied by intensity-modulated photocurrent spectroscopy. *Journal of Electroanalytical Chemistry* **2020,** *860*, 113891.
52. Hautier, G.; Miglio, A.; Waroquiers, D.; Rignanese, G.-M.; Gonze, X., How Does Chemistry Influence Electron Effective Mass in Oxides? A High-Throughput Computational Analysis. *Chemistry of Materials* **2014,** *26* (19), 5447-5458.
53. Ju, S.; Cai, T.-Y., Magnetic and optical anomalies in infinite-layer iron oxide CaFeO2 and BaFeO2: A density functional theory investigation. *Journal of Applied Physics* **2009,** *106* (9).
54. Tassel, C.; Pruneda, J. M.; Hayashi, N.; Watanabe, T.; Kitada, A.; Tsujimoto, Y.; Kageyama, H.; Yoshimura, K.; Takano, M.; Nishi, M.; Ohoyama, K.; Mizumaki, M.; Kawamura, N.; Íñiguez, J.; Canadell, E., CaFeO2: A New Type of Layered Structure with Iron in a Distorted Square Planar Coordination. *Journal of the American Chemical Society* **2009,** *131* (1), 221-229.
55. Gupta, M. K.; Mittal, R.; Chaplot, S. L.; Tassel, C.; Kageyama, H.; Tomiyasu, K.; Taylor, J., Phonons and stability of infinite-layer iron oxides SrFeO2 and CaFeO2. *Solid State Communications* **2016,** *241*, 43-55.
56. Kageyama, H.; Hayashi, K.; Maeda, K.; Attfield, J. P.; Hiroi, Z.; Rondinelli, J. M.; Poeppelmeier, K. R., Expanding frontiers in materials chemistry and physics with multiple anions. *Nature Communications* **2018,** *9*.
57. Almoussawi, B.; Kageyama, H.; Roussel, P.; Kabbour, H., Versatile Interplay of Chalcogenide and Dichalcogenide Anions in the Thiovanadate Ba7S(VS3O)2(S2)3 and Its Selenide Derivatives: Elaboration and DFT Meta-GGA Study. *ACS Organic & Inorganic Au* **2023,** *3* (3), 158-170.
58. Yu, L.; Wang, L.; Dou, Y.; Zhang, Y.; Li, P.; Li, J.; Wei, W., Recent Advances in Ferroelectric Materials-Based Photoelectrochemical Reaction. *Nanomaterials* **2022,** *12* (17), 3026.
59. Jaulmes, S., Oxysulfure de gallium et de lanthane LaGaOS2. *Acta Crystallographica Section B* **1978,** *34* (8), 2610-2612.

60. Ogisu, K.; Ishikawa, A.; Shimodaira, Y.; Takata, T.; Kobayashi, H.; Domen, K., Electronic Band Structures and Photochemical Properties of La−Ga-based Oxysulfides. *The Journal of Physical Chemistry C* **2008,** *112* (31), 11978-11984.
61. Clarke, S. J.; Adamson, P.; Herkelrath, S. J. C.; Rutt, O. J.; Parker, D. R.; Pitcher, M. J.; Smura, C. F., Structures, Physical Properties, and Chemistry of Layered Oxychalcogenides and Oxypnictides. *Inorganic Chemistry* **2008,** *47* (19), 8473-8486.
62. Tributsch, H., Hole Reactions from d-Energy Bands of Layer Type Group VI Transition Metal Dichalcogenides: New Perspectives for Electrochemical Solar Energy Conversion. *Journal of The Electrochemical Society* **1978,** *125* (7), 1086.
63. Kam, K. K.; Parkinson, B. A., Detailed photocurrent spectroscopy of the semiconducting group VIB transition metal dichalcogenides. *The Journal of Physical Chemistry* **1982,** *86* (4), 463-467.
64. Hamilton, J. W. J.; Byrne, J. A.; McCullagh, C.; Dunlop, P. S. M., Electrochemical Investigation of Doped Titanium Dioxide. *International Journal of Photoenergy* **2008,** *2008*, 631597.
65. Wang, Y.; Huang, J.; Wang, L.; She, H.; Wang, Q., Research progress of ferrite materials for photoelectrochemical water splitting. *Chin. J. Struct. Chem.* **2022,** *41*, 2201054-2201068.
66. Wang, L.; Zhang, J.; Li, Y.; Shi, Y.; Huang, J.; Mei, Q.; Wang, L.; Ding, F.; Bai, B.; Wang, Q., Heterostructured CoFe1.5Cr0.5S3O/COFs/BiVO4 photoanode boosts charge extraction for efficient photoelectrochemical water splitting. *Applied Catalysis B: Environmental* **2023,** *336*, 122921.